Supplementary information

Title: Locating Manganese Vanadate Phase with PO_4^{3-}-Modified Mn^{2+}-O-V^{5+} Motifs Optimized for Catalytic NO_X and Poison Abatement under Oxidative Wet Conditions

Authors: Seokhyun Lee,[a] So Hyeon Park,[b] and Jongsik Kim [b, c] *

* corresponding author: jkim40@khu.ac.kr (J. Kim)

Affiliations:

[a] Ajou Energy Science Research Center, Ajou University, Suwon, 16499, South Korea.

[b] Department of Chemical Engineering (Integrated Engineering Program), Kyung Hee University, Yongin, 17104, South Korea.

[c] KHU-KIST Department of Converging Science and Technology, Kyung Hee University, Seoul, 02447, South Korea.

Contents

Experimental section

Catalysts

The catalysts were synthesized via impregnation-calcination techniques according to the protocols with minor modifications from those we reported earlier.[1-8] In the typical synthesis of TiO_2-supported $Mn_XV_2O_{X+5}$ (X=1, 2, or 3; referred to as Mn_X), 1.96 mmol of NH_4VO_3 (Junsei; ≥99.0 %) dissolved in 140 mL de-ionized H_2O was mixed with 'Z' mmol of $Mn(NO_3)_2 \bullet XH_2O$ (Sigma-Aldrich; 98.0 %) dissolved in 60 mL de-ionized H_2O ('Z' of 0.98 mmol for Mn_1; 1.96 mmol for Mn_2; 2.94 mmol for Mn_3), stirred at 25 °C for an hour, and further mixed with 'W' g of TiO_2 (DT51 (anatase); CristalACTiV^{TM}; 'W' g of 4.85 g for Mn_1; 4.79 g for Mn_2; 4.74 g for Mn_3) prior to being stirred at 25 °C for 18 hours.[1-6] The resulting synthetic mixture was then subjected to rotary evaporation for the removal of H_2O, dried overnight at 110 °C, and calcined at 500 °C for 5 hours with the ramping rate of 5 °C min^{-1}.[1-6] In the typical synthesis of TiO_2-supported Sb_2O_5 (referred to as Sb_2O_5/TiO_2), 7.39 mmol of $Sb(CH_3COO)_3$ (Alfa Aesar; 97.0 %) was dissolved in 250 mL of CH_3COOH (J. T. Baker; ≥97.0 %), mixed with 29.1 g of DT51, stirred at 25 °C for 18 hours, subjected to rotary evaporation for the removal of CH_3COOH, dried overnight at 110 °C, and calcined at 500 °C for 5 hours with the ramping rate of 5 °C min^{-1}.[1-6] In the typical synthesis of Sb_2O_5-promoted Mn_1 (referred to as Mn_1-Sb), its procedures were identical to those used to synthesize Mn_1 except for the substitution of 4.85 g of Sb_2O_5/TiO_2 for 4.85 g of TiO_2.[1-6] In the typical synthesis of Mn_X (or Mn_1-Sb) modified with (protonated) PO_4^{3-} functionalities (referred to as Mn_X-P (or Mn_1-Sb-P)), 0.44 mmol of $(NH_4)_2HPO_4$ (Daejung; ≥98.5 %) was dissolved in 250 mL de-ionized H_2O, mixed with 3 g of Mn_X (or Mn_1-Sb), stirred at 25 °C for 18 hours, subjected to rotary evaporation for the removal of H_2O, dried overnight at 110 °C, and calcined at 500 °C for an hour with the ramping rate of 10 °C min^{-1}.[7, 8] In the typical synthesis of Mn_1-Sb modified with (protonated) SO_A^{2-} (A=3-4) functionalities (referred to as Mn_1-Sb-S), Mn_1-Sb was exposed to a N_2-balanced gas including 500 ppm SO_2 and 3 vol. % O_2/N_2 at 500 °C for an hour with the ramping rate of 10 °C min^{-1} and the flow rate of 500 mL min^{-1}.[1, 2] A commercial control of WO_3-promoted V_2O_5 on TiO_2 (referred to as V_2O_5-WO_3) was synthesized according to the protocols we reported elsewhere.[1-6] Mn_1-Sb-S and V_2O_5-WO_3 were utilized for comparison with Mn_1-Sb-P.

Characterizations

A NOVA 2200e (Quantachrome Instruments) served to collect N_2 adsorption-desorption isotherms of the catalysts at -196 °C after their surfaces were purged under vacuum (1.0X10^{-3} mmHg) at 150 °C for 3 hours. The volumes of N_2 adsorbed in a-per gram of the catalysts at partial pressure regimes (P/P$_0$) of 0.05-0.30 were considered to evaluate their N_2-accessible Brunauer-Emmett-Teller (BET) surface areas ($S_{BET, N2}$) and Barrett-Joyner-Halenda (BJH) pore volumes ($V_{BJH, N2}$) at -196 °C. A BELSORP-MAX (MicrotracBEL Corp.) served to collect H_2O adsorption isotherms of the catalysts at 10-40 °C after their surfaces were purged under vacuum (1.0X10^{-3} mmHg) at 150 °C for 3 hours.[4, 6, 9-13] The amounts of H_2O adsorbed in a-per gram of the catalysts (N_{H2O}) at partial pressure regimes (P/P$_0$) of 0.05-0.30 were considered to assess their H_2O-accessible BET surface areas ($S_{BET, H2O}$) at 10-40 °C.[4, 6, 9-13] Moreover, H_2O adsorption isotherms were simulated via Toth fitting (Eqn. S1), in which δ is referred to as the maximum number of H_2O adsorbed in a per-gram of the catalyst (mol$_{H2O}$ g$_{CAT}^{-1}$), whereas ε, ζ, and P are referred to as the constant indigenous to the catalyst (bar^{-1}), the constant concerning heterogeneous feature of the catalyst surface (dimensionless-less), and the pressure (bar), respectively.[4, 6, 9-13] Isosteric heats of H_2O adsorption on the catalyst surfaces at near-zero H_2O coverages (E_{H2O}) were then evaluated with the use of Clausius-Clapeyron equation (Eqn. S2), in which P_1/P_2 and R are referred to as the pressures (bar) at the temperatures of T_1/T_2 (K) and the ideal gas constant (8.3145 J mol^{-1} K^{-1}), respectively.[4, 6, 9-13]

$$N_{H2O} = \delta \times \frac{\varepsilon \times P}{(1 + (\varepsilon \times P)^\zeta)^{\left(\frac{1}{\zeta}\right)}} \quad (S1)$$

$$ln\left(\frac{P_1}{P_2}\right) = \frac{E_{H2O}}{R} \times \left(\frac{T_1 - T_2}{T_1 \times T_2}\right) \quad (S2)$$

An ICS 3000 (Thermo Fisher Scientific) served to carry out inductively coupled plasma-optical emission spectroscopy (ICP-OES) and inductively coupled plasma-atomic absorption spectroscopy (ICP-AAS) experiments of the catalysts. An Ultim max 170 (Oxford) served to collect energy-dispersive X-ray spectroscopy (EDX) mapping images of the catalysts at the acceleration voltage of 15 keV after their surfaces were purged under vacuum (1.0X10^{-6} mmHg). A Titan 80-300^{TM} (FEI) served to collect high-resolution transmission electron microscopy (HRTEM) images and selected area electron diffraction (SAED) patterns of the catalysts at the acceleration voltage of 300 keV after their surfaces were purged at 25 °C under vacuum (2.0X10^{-7} mmHg). A D8 Advance diffractometer (Bruker) served to collect X-ray diffraction (XRD) patterns of the catalysts under analytic

conditions of the 2θ range, the step size, and the scan speed of 20°-80°, 0.02° per step, and 2 seconds per step, respectively, with the use of Cu K_α radiation (λ = 1.54 Å). A PHI 5000 VersaProbe (Ulvac-Phi) served to collect X-ray photoelectron (XP) spectra of the catalysts and their surface atomic concentrations after the catalyst surfaces were purged at 25 °C under vacuum (1.5×10^{-10} mmHg). The XP spectra provided the resolution of 0.1 eV and were de-convoluted using Gaussian functions.[1-8, 14] A Varian 400 MHz solid NMR spectrometer (Agilent Technologies) coupled with a 4.0 mm NB probe served to collect ^{31}P magic angle spinning (MAS) nuclear magnetic resonance (NMR) spectra of the catalysts with the channel of a 4.0 mm NB probe being dialed in to 161.97 MHz at the temperature and the magnetic field of 25 °C and 9.39 T, respectively.[7, 8, 10] The ^{31}P MAS NMR spectra of the catalysts loaded in a ZrO_2 rotor with the outer radius of 4.0 mm were collected under analytic conditions of the π/2 signal duration, the acquisition time, the total scan number, the spinning rate, and the recycle delay of 4.0 μsecond, 0.02 second, 10,000, 10.0 kHz, and 0.2 μsecond, respectively.[7, 8, 10] The ^{31}P MAS NMR spectra were de-convoluted using Gaussian functions.[7, 8, 10] An FT/IR-6X (Jasco) equipped with ZnSe optics and a mercury-cadmium-telluride detector served to monitor background-subtracted, *in situ* diffuse reflectance infrared Fourier transform (DRIFT) spectra for the catalysts with their surfaces being purged under 3 vol. % O_2/N_2 at 300 °C for 30 minutes and exposed to a N_2-balanced feed gas containing 1,000 ppm NH_3 or 1,000 ppm $NO/3.0$ vol. % O_2 at 220 °C for 30 minutes (Fig. 5).[1-8, 14] A BELCAT-B (BEL Japan, Inc.) served to collect the profiles of CO-pulsed chemisorption (thermal conductivity detector (TCD) signal *versus* time), O_2-pulsed chemisorption (thermal conductivity detector (TCD) signal *versus* time), H_2-temperature-programmed reduction (H_2-TPR; thermal conductivity detector (TCD) signal *versus* temperature), NH_3-temperature-programmed desorption (NH_3-TPD; thermal conductivity detector (TCD) signal *versus* temperature), and O_2-temperature-programmed desorption (O_2-TPD; thermal conductivity detector (TCD) signal *versus* temperature) for the catalysts. CO-pulsed chemisorption experiments were conducted by letting the catalyst surfaces be purged under 10 vol. % O_2/He at 300 °C for an hour, cooled to 50 °C under a He, and subjected to periodic CO injection at 50 °C until the CO pulse-induced change in thermal conductivity detector (TCD) signals was minute.[1-8, 14] O_2-pulsed chemisorption experiments were performed by letting the catalyst surfaces be purged under 10 vol. % O_2/He at 300 °C for an hour, cooled to 50 °C under a He, reduced under 10 vol. % H_2/He at 300 °C for an hour with the ramping rate of 10 °C min^{-1}, cooled to 250 °C under a He, and subjected to periodic O_2 injection at 250 °C until the O_2 pulse-induced change in thermal conductivity detector (TCD) signals was minute.[3-6] H_2-TPR experiments were carried out by letting the catalyst surfaces be purged under an Ar at 300 °C for an hour, cooled to 50 °C under an Ar, and heated to 800 °C under 10 vol. % H_2/Ar with the ramping rate of 10 °C min^{-1}. NH_3-TPD experiments were conducted by letting the catalyst surfaces be purged under 10 vol. % O_2/He at 300 °C for an hour, cooled to 50 °C (or 220 °C) under a He, and exposed to 5 vol. % NH_3/He at 50 °C (or 220 °C) for an hour to saturate the surfaces with NH_3.[1-8, 14] The surfaces were then exposed to a He at 50 °C (or 220 °C) for an hour to remove physisorbed NH_3 molecules and heated to 700 °C under a He with the ramping rates (β) of 10 (for NH_3 chemisorption at 50 °C) or 10-30 °C min^{-1} (for NH_3 chemisorption at 220 °C).[1-8, 14] The resulting NH_3-TPD profile at a β value was then de-convoluted using Gaussian functions to provide three sub-bands (I-III), each of which possessed the temperature with the maximum intensity of TCD signal (T_{MAX}).[1-8, 14] Eqn. S3 then served to evaluate the energy required to release NH_3 molecules from the catalyst surface (E_{NH3}) at 220 °C via TPD theory.[1-8] In Eqn. S3, $θ_{MAX}$ and v_n/n correspond to the surface coverage of NH_3 at T_{MAX} and the lumped constants indigenous to the surface, respectively.[1-8, 14]

$$ln\left(\frac{\beta}{T_{MAX}^2}\right) = -\left(\frac{E_{NH3}}{R}\right)\left(\frac{1}{T_{MAX}}\right) - \underbrace{2.303 \times \log\left(\frac{E_{NH3}}{v_n Rn\theta_{MAX}^{n-1}}\right)}_{CONSTANT} \quad (S3)$$

O_2-TPD experiments were conducted by letting the catalyst surfaces be purged under 10 vol. % O_2/He at 300 °C for an hour, cooled to 50 °C under a He, and reduced using 10 vol. % H_2/He at 300 °C for an hour with the ramping rate of 10 °C min^{-1}.[3-6] The surfaces were then cooled to 50 °C under a He, exposed to 3 vol. % O_2/He at 50 °C for an hour, exposed to a He at 50 °C for an hour to remove physisorbed O_2 molecules, and heated to 700 °C under a He with the β values of 10-30 °C min^{-1}.[3-6] The resulting O_2-TPD profile at a β value was then de-convoluted using Gaussian functions to provide three sub-bands (I-III), each of which possessed the temperature with the maximum intensity of TCD signal (T_{MAX}).[3-6] Eqn. S4 then served to evaluate the energy required to release mobile oxygens (O_M) from the catalyst surface (E_{OM}) at 50 °C via TPD theory. In Eqn. S4, $θ_{MAX}$ and v_n/n correspond to the surface coverage of O_2 at T_{MAX} and the lumped constants indigenous to the surface, respectively.[3-6]

$$ln\left(\frac{\beta}{T_{MAX}^2}\right) = -\left(\frac{E_{OM}}{R}\right)\left(\frac{1}{T_{MAX}}\right) - \underbrace{2.303 \times \log\left(\frac{E_{OM}}{v_n Rn\theta_{MAX}^{n-1}}\right)}_{CONSTANT} \quad (S4)$$

A quartz reactor equipped with a SO$_2$ analyzer (Fuji Electric Co., ZKJ-2) served to collect the profiles of SO$_2$-TPD (SO$_2$ concentration (C_{SO2}) *versus* temperature) for the catalysts by letting the catalyst surfaces be purged under 3 vol. % O$_2$/N$_2$ at 300 °C for an hour, cooled to 220 °C under a N$_2$, and exposed to 5,000 ppm SO$_2$/N$_2$ at 220 °C for an hour to saturate the surfaces with SO$_2$ molecules.[3-6] The surfaces were then exposed to a N$_2$ at 220 °C for an hour to remove physisorbed SO$_2$ molecules and heated to 900 °C under a N$_2$ with β values of 10-20 °C min^{-1}.[3-6] The resulting SO$_2$-TPD profile at a β value was then de-convoluted using Gaussian functions to provide five sub-bands (I-V), each of which possessed the temperature with the maximum intensity of C_{SO2} (T_{MAX}).[3-6] Eqn. S5 then served to evaluate the energy required to release SO$_2$ molecules from the catalyst surface (E_{SO2}) at 220 °C via TPD theory.[3-6] In Eqn. S5, θ_{MAX} and v_n/n correspond to the surface coverage of SO$_2$ at T_{MAX} and the lumped constants indigenous to the surface, respectively.[3-6]

$$ ln\left(\frac{\beta}{T_{MAX}^2}\right) = -\left(\frac{E_{SO2}}{R}\right)\left(\frac{1}{T_{MAX}}\right) - \underbrace{2.303 \times \log\left(\frac{E_{SO2}}{v_n R n \theta_{MAX}^{n-1}}\right)}_{CONSTANT} \quad (S5) $$

A thermo-gravimetric analyzer (TGA, Mettler Toledo, TGA 2) connected to a mass spectrometer (MASS, Hiden Analytical, HPR20) served to collect the profiles of weight percent (W; wt. %) loss *versus* temperature and SO$_2$ signal (m/z~64) released *versus* temperature for the catalysts poisoned with ammonium sulfate (AS) and ammonium bisulfate (ABS).[1, 2, 4-6] Typically, the AS/ABS-poisoned catalyst was loaded in an Al$_2$O$_3$ pans, purged under an Ar at 100 °C for an hour to remove physisorbed H$_2$O molecules, and heated to 600 °C under an Ar with the ramping rate of 5 °C min^{-1} and the flow rate of 50 mL min^{-1}.[1, 2, 4-6]

Reactions

The catalyst particulates sieved with sizes of 200-300 μm or 300-425 μm were loaded in a quartz reactor with an inner diameter of 0.6 cm or 0.8 cm and altered the reaction control volume of 0.066-0.50 mL at the total flow rate of 500 mL min^{-1}, leading to achieve the gas hourly space velocities (GHSV) of 60,000-450,000 hr^{-1}.[1-8, 14] In the typical selective catalytic NO$_X$ reduction (SCR) run, a quartz reactor bearing the catalyst particulates was situated inside a furnace, purged under 3 vol. % O$_2$/N$_2$ at 500 °C for an hour, and exposed to a N$_2$-balanced, wet feed gas composed of 800 ppm NO$_X$, 800 ppm NH$_3$, 3.0 vol. % O$_2$, 5.4 vol. % H$_2$O, or 500 ppm SO$_2$ at 150-400 °C with the total flow rate of 500 mL min^{-1}.[1-8, 14] A gas component downstream of a quartz reactor was quantified using a ZKJ-2 (Fuji Electric Co.) and a detector tube (GASTEC Co.) for NO/N$_2$O/O$_2$/SO$_2$ and for NO$_2$/NH$_3$, respectively.[1-8, 14] Eqn. S6 and S7 served to evaluate NO$_X$ conversion (X_{NOX}) and N$_2$ selectivity (S_{N2}) for the catalyst, respectively. In Eqn. S6-S7, $C_{j, IN}$ and $C_{j, OUT}$ are referred to as the concentration of gaseous species j at the inlet (IN) and the outlet (OUT), respectively.[1-8, 14]

$$ X_{NOX}\ (\%) = \frac{C_{NOX,IN} - C_{NOX,OUT}}{C_{NOX,IN}} \times 100 \quad (S6) $$

$$ S_{N2}\ (\%) = \frac{C_{NO,IN} + C_{NH3,IN} - C_{NO,OUT} - C_{NH3,OUT} - C_{NO2,OUT} - 2 \times C_{N2O,OUT}}{C_{NO,IN} + C_{NH3,IN} - C_{NO,OUT} - C_{NH3,OUT}} \times 100 \quad (S7) $$

Eqn. S8 served to assess NO$_X$ consumption rate of the catalyst defined by the moles of NO$_X$ consumed in a per-BA$^-$-H$^+$ site and in a per-unit time basis (-r_{NOX}).[1-6, 8, 14] In Eqn. S8, N_{NH3} is referred to as the amount of NH$_3$ chemisorbed in a per-gram of the catalyst at 220 °C, as determined via its NH$_3$-TPD experiment (Fig. S6-S7).[1-6, 8, 14]

$$ -r_{NOX}\ (min^{-1}) = \frac{moles\ of\ NO_X\ consumed\ in\ a\ per-gram\ of\ the\ catalyst\ and\ in\ a\ per-unit\ time\ basis\ (\Delta mol_{NOX}\ g_{CAT}^{-1}\ min^{-1})}{N_{NH3}\ of\ the\ catalyst\ (mol_{NH3}\ g_{CAT}^{-1})} \quad (S8) $$

Eqn. S9 served to assess ABS consumption rate of the catalyst defined by the moles of ABS consumed in a per-BA$^-$-H$^+$ site and in a per-unit time basis (-r_{ABS}).[1, 2, 4-6] In Eqn. S9, N_{NH3} is referred to as the amount of NH$_3$ chemisorbed in a per-gram of the catalyst at 220 °C, as determined via its NH$_3$-TPD experiment (Fig. S6-S7).[1, 2, 4-6] Moreover, in Eqn. S9, moles of ABS consumed in a per-gram of the catalyst ($\Delta mol_{ABS}\ g_{CAT}^{-1}$) and time span (Δt) required to quantify $\Delta mol_{ABS}\ g_{CAT}^{-1}$ is determined via TGA-MASS dataset of the catalyst at 260 (<±0.3) °C, 270 (<±0.3) °C, 280 (<±0.3) °C, and 290 (<±0.3) °C.[1, 2, 4-6]

$$ -r_{ABS}\ (min^{-1}) = \frac{moles\ of\ ABS\ consumed\ in\ a\ per-gram\ of\ the\ catalyst\ (\Delta mol_{ABS}\ g_{CAT}^{-1})}{N_{NH3}\ of\ the\ catalyst\ (mol_{NH3}\ g_{CAT}^{-1}) \times\ time\ span\ (\Delta t)\ required\ to\ quantify\ \Delta mol_{ABS}\ g_{CAT}^{-1}\ (min)} \quad (S9) $$

Table S1. The numbers of V^{5+}-O-Mn^{2+} channels in a per-Mn^{2+} center ($N_{V5+\text{-}O\text{-}Mn2+}$) pertaining to $[Mn^{2+}\text{-}(O^{2-})_6]^{10-}$ sub-units for intact $Mn_XV_2O_{X+5}$ architectures.

X	geometry of sub-unit [a]	coordination number of Mn^{2+} center [a]	bridged bond (type; number) [a]	$N_{V5+\text{-}O\text{-}Mn2+}$ [a]
1	*octahedral*	6	■ Mn^{2+}/V^{5+}-O-Mn^{2+} (*bi-*; 4) ■ V^{5+}/V^{5+}-O-Mn^{2+} (*bi-*; 2)	8
2	*octahedral*	6	■ Mn^{2+}/V^{5+}-O-Mn^{2+} (*bi-*; 4) ■ $Mn^{2+}/V^{5+}/V^{5+}$-O-Mn^{2+} (*tri-*; 2)	8
3	*octahedral*	6	■ Mn^{2+}/V^{5+}-O-Mn^{2+} (*bi-*; 4) ■ $Mn^{2+}/Mn^{2+}/V^{5+}$-O-Mn^{2+} (*tri-*; 2)	6

[a] See Fig. 1D-1F.

Table S2. The numbers of Mn^{2+}-O-V^{5+} channels in a per-V^{5+} center ($N_{Mn2+-O-V5+}$) pertaining to $[V^{5+}-(O^{2-})_6]^{7-}$ and $[V^{5+}-(O^{2-})_4]^{3-}$ sub-units for intact $Mn_XV_2O_{X+5}$ architectures with X values of 1 and ≥2, respectively.

X	geometry of sub-unit [a]	coordination number of V^{5+} center [a]	bridged bond (type; number) [a]	$N_{Mn2+-O-V5+}$ [a]
1	*octahedral*	6	■ V^{5+}/V^{5+}-O-V^{5+} (*bi-*; 3) ■ V^{5+}/Mn^{2+}-O-V^{5+} (*bi-*; 2) ■ Mn^{2+}/Mn^{2+}-O-V^{5+} (*bi-*; 1)	4
2	*tetrahedral*	4	■ V^{5+}-O-V^{5+} (*non-*; 1) ■ Mn^{2+}/Mn^{2+}-O-V^{5+} (*bi-*; 3)	6
3	*tetrahedral*	4	■ Mn^{2+}/Mn^{2+}-O-V^{5+} (*bi-*; 3) ■ $Mn^{2+}/Mn^{2+}/Mn^{2+}$-O-V^{5+} (*tri-*; 1)	9

[a] See Fig. 1D-1F.

Table S3. The hierarchies predicted concerning the properties of $Mn_XV_2O_{X+5}$ architectures (X=1-3) with the use of their $N_{V5+-O-Mn2+}$ or $N_{Mn2+-O-V5+}$ values and those identified for the Mn_X catalysts via experiments.

	anticipated for $Mn_XV_2O_{X+5}$						identified for Mn_X
	$N_{V5+-O-Mn2+}$			$N_{Mn2+-O-V5+}$			experimental result
X	1	2	3	1	2	3	-
$N_{V5+-O-Mn2+}$ (or $N_{Mn2+-O-V5+}$)	8	8	6	4	6	8	
N_{NH3}	X of 1~2>3			X of 1<2<3			1~2<3 [a]
$k'_{APP,0}$	X of 1~2>3			X of 1<2<3			1~2<3 [b]
E_{NH3}	X of 1~2<3			X of 1>2>3			1~2<3 [a]
$E_{BARRIER}$	X of 1~2<3			X of 1>2>3			1~2<3 [b]
N_{OL}	X of 1~2>3			-			1~2>3 [c]
E_{OL}	-			X of 1<2<3			1~2<3 [c]
N_{OM} (~N_{OV})	X of 1~2>3			-			1~2>3 [d]
E_{OM}	X of 1~2<3			X of 1>2>3			1~2<3 [d]
O_M mobility	X of 1~2>3			X of 1<2<3			1~2>3 [d]

[a] via NH_3-TPD (Fig. 4A, Fig. S6-S7, and Table S7). [b] via Arrhenius plot (Fig. 4C). [c] via XP spectroscopy (Fig. S8 and Table S5). [d] via O_2-pulsed chemisorption (Table S4) or O_2-TPD (Fig. 6A, Fig. S10-S11, and Table S9).

Table S4. Properties of the catalysts.

	Mn$_1$	Mn$_2$	Mn$_3$	Mn$_1$-Sb	Mn$_1$-P	Mn$_2$-P	Mn$_3$-P	Mn$_1$-Sb -P
$S_{BET, N2}$ [a, b] (m$_{N2}^2$ g$_{CAT}^{-1}$)	-	-	-	-	76.5 (±4.2)	74.9 (±3.5)	74.9 (±4.8)	70.9 (±3.5)
$V_{BJH, N2}$ [a, c] (cm$_{N2}^3$ g$_{CAT}^{-1}$)	-	-	-	-	0.3 (±0.1)	0.3 (±0.1)	0.3 (±0.1)	0.3 (±0.1)
Mn/V (bulk) [d, e, f]	-	-	-	-	0.5 (±0.1)	1.0 (±0.1)	1.4 (±0.1)	0.5 (±0.1)
Mn/V (surface) [d, g]	-	-	-	-	0.2 (±0.1)	0.4 (±0.1)	0.7 (±0.1)	0.2 (±0.1)
Mn/V (surface) [d, h]	-	-	-	-	0.2 (±0.1)	0.4 (±0.1)	0.7 (±0.1)	0.2 (±0.1)
P/metal (bulk) [d, e, f, i]	-	-	-	-	0.3 (±0.1)	0.2 (±0.1)	0.2 (±0.1)	0.2 (±0.1)
P/metal (surface) [d, g, i]	-	-	-	-	0.7 (±0.1)	0.6 (±0.1)	0.7 (±0.1)	0.7 (±0.1)
P/metal (surface) [d, h, i]	-	-	-	-	0.7 (±0.1)	0.7 (±0.1)	0.7 (±0.1)	0.7 (±0.1)
metal/V (surface) [d, g, i]	-	-	-	-	0.2 (±0.1)	0.4 (±0.1)	0.7 (±0.1)	0.6 (±0.1)
metal/V (surface) [d, h, i]	-	-	-	-	0.2 (±0.1)	0.4 (±0.1)	0.7 (±0.1)	0.6 (±0.1)
N_{CO} [j] (X10^{-1} µmol$_{CO}$ g$_{CAT}^{-1}$)	2.1 (±0.1)	5.4 (±0.3)	5.0 (±0.3)	2.8 (±0.1)	1.7 (±0.1)	4.2 (±0.2)	4.4 (±0.1)	2.4 (±0.1)
N_{O2} [k] (µmol$_{O2}$ g$_{CAT}^{-1}$)	-	-	-	-	27.3 (±2.0)	29.5 (±2.6)	21.5 (±1.8)	27.2 (±2.4)

[a] via N$_2$ physisortion at -196 °C. [b] via BET theory. [c] via BJH theory. [d] molar ratio. [e] via ICP-OES. [f] via ICP-AAS. [g] via XP spectroscopy. [h] via EDX mapping. [i] metal of Mn+V for Mn$_x$-P; Mn+V+Sb for Mn$_1$-Sb-P. [j] via CO-pulsed chemisorption at 50 °C. [k] via O$_2$-pulsed chemisorption at 250 °C.

Table S5. Locations and compositions of phases present in the catalyst surfaces examined via XP spectra.

region	phase	Mn$_1$-P		Mn$_2$-P		Mn$_3$-P		Mn$_1$-Sb-P	
		location (eV)	composition (%)	location (eV)	composition (%)	location (eV)	composition (%)	location (eV)	composition (%)
Mn 2p $_{1/2}$ $^{a, b, c}$	Mn^{2+} (●)	652.3	41.2	652.3	28.6	652.7	28.2	652.0	36.1
	Mn^{3+} (●)	653.7	36.7	653.7	32.6	654.1	48.4	653.4	33.8
	Mn^{4+} (●)	655.5	22.1	655.5	38.8	655.9	23.4	655.2	30.1
Mn 2p $_{3/2}$ $^{a, b, c}$	Mn^{2+} (○)	640.9	41.2	640.9	28.6	641.3	28.2	640.6	36.1
	Mn^{3+} (○)	642.0	36.7	642.0	32.6	642.4	48.4	641.7	33.8
	Mn^{4+} (○)	643.5	22.1	643.5	38.8	643.9	23.4	643.2	30.1
V 2p $_{3/2}$ $^{a, b, d}$	V^{3+} (○)	515.6	35.2	515.3	19.1	515.0	7.0	515.9	49.5
	V^{4+} (○)	516.6	21.9	516.3	33.3	516.0	16.4	516.9	26.4
	V^{5+} (○)	517.3	42.9	517.0	47.6	516.7	76.6	517.6	24.1
P 2p $_{3/2}$ $^{a, b, e}$	PO$_4$$^{3-}$ (○)	131.7	11.2	131.7	11.4	131.7	10.9	131.7	11.8
	HPO$_4$$^{2-}$ (○)	132.7	8.1	132.7	9.6	132.7	9.5	132.7	8.5
	H$_2$PO$_4$$^{-}$ (○)	133.6	80.7	133.6	79.0	133.6	79.6	133.6	79.7
O 1s $^{a, b, f}$	O$_\beta$ (○)	529.9	64.6	529.9	67.1	529.9	71.0	530.0	63.1
	O$_\alpha$ (○)	530.5	30.4	530.5	29.9	530.3	24.2	530.7	34.1
	O$_\alpha$' (○)	532.0	5.0	532.0	3.0	532.0	4.8	532.0	2.8

^{a} de-convoluted using Gaussian functions. ^{b} peak resolution of 0.1 eV. ^{c} See Fig. S3. ^{d} See Fig. S4. ^{e} See Fig. 3A-3D. ^{f} See Fig. S8.

Table S6. Locations and compositions of PO_4^{3-} modifier and its protonated analogues present in the catalyst surfaces examined via ^{31}P MAS NMR spectra.

functionality	Mn$_1$-P location (ppm)	Mn$_1$-P composition (%)	Mn$_2$-P location (ppm)	Mn$_2$-P composition (%)	Mn$_3$-P location (ppm)	Mn$_3$-P composition (%)	Mn$_1$-Sb-P location (ppm)	Mn$_1$-Sb-P composition (%)
PO_4^{3-} (o) [a, b]	-24.6	11.5	-24.6	11.8	-24.6	11.0	-24.6	11.3
HPO_4^{2-} (o) [a, b]	-17.6	7.7	-17.6	9.8	-17.6	9.1	-17.6	8.5
$H_2PO_4^-$ (o) [a, b]	-10.6	80.8	-10.6	78.4	-10.6	79.9	-10.6	80.2

[a] de-convoluted using Gaussian functions. [b] See Fig. 3E-3H.

Table S7. T_{MAX} values and slopes of ln (β/T_{MAX}^2) *versus* $1/T_{MAX}$ for the sub-bands pertaining to the de-convoluted NH_3-TPD profiles of the catalysts recorded post NH_3 chemisorption at 220 °C with β values of 10-30 °C min^{-1}.

sub-band	β (°C min^{-1})	T_{MAX} (°C)			
		Mn_1-P	Mn_2-P	Mn_3-P	Mn_1-Sb- P
I [a, b]	10	346.4	337.2	370.3	362.3
	20	350.0	340.0	373.2	366.0
	30	352.7	342.8	376.0	369.4
II [a, b]	10	403.3	403.6	417.5	396.2
	20	407.2	407.0	420.7	400.6
	30	410.5	410.3	424.0	403.8
III [a, b]	10	483.0	499.9	522.1	452.6
	20	487.0	504.0	526.0	457.0
	30	491.4	508.4	530.4	461.2

sub-band	slope [d, e] (K)			
	Mn_1-P	Mn_2-P	Mn_3-P	Mn_1-Sb- P
I [c]	-2928.5	-3355.7	-3673.2	-3645.2
II [c]	-3014.5	-3380.0	-3667.4	-2690.9
III [c]	-3172.6	-3294.4	-3648.9	-2769.1

[a] de-convoluted using Gaussian functions. [b] See Fig. S6-S7. [c] See Fig. 4A. [d] via TPD theory. [e] regression factors (R^2) of ≥0.99.

Table S8. $-r_{NOX}$ values of the catalysts recorded at 205-250 °C.

$T_{REACTION}$ (°C)	$-r_{NOX}$ [a, b, c] ($X10^{-1}$ min^{-1})			
	Mn$_1$-P	Mn$_2$-P	Mn$_3$-P	Mn$_1$-Sb- P
205	1.9 (±0.1)	1.8 (±0.1)	1.1 (±0.1)	2.1 (±0.1)
220	2.7 (±0.1)	2.7 (±0.1)	1.6 (±0.1)	3.0 (±0.1)
235	4.0 (±0.1)	4.0 (±0.3)	2.6 (±0.1)	4.3 (±0.1)
250	5.5 (±0.1)	5.3 (±0.1)	3.4 (±0.1)	6.2 (±0.1)

[a] SCR environments: 800 ppm NO_X; 800 ppm NH_3; 3.0 vol. % O_2; 5.4 vol. % H_2O; catalyst sieved with sizes of 300-425 μm; GHSV of 350,000 hr^{-1}; total flow rate of 500 mL min^{-1}; balanced by a N_2. [b] X_{NOX} values of <30.0 %. c S_{N2} values of ~100.0 %.

Table S9. T_{MAX} values and slopes of $\ln(\beta/T_{MAX}^2)$ *versus* $1/T_{MAX}$ for the sub-bands pertaining to the de-convoluted O_2-TPD profiles of the catalysts recorded post O_2 chemisorption at 50 °C with β values of 10-30 °C min^{-1}.

sub-band	β (°C min^{-1})	T_{MAX} (°C)			
		Mn$_1$-P	Mn$_2$-P	Mn$_3$-P	Mn$_1$-Sb- P
I [a, b]	10	290.2	302.9	312.0	232.6
	20	293.0	305.4	314.8	235.0
	30	295.2	308.5	317.0	237.4
II [a, b]	10	443.5	419.6	398.2	364.8
	20	447.6	423.5	401.8	368.4
	30	451.6	426.8	404.6	372.0
III [a, b]	10	488.1	485.9	465.4	487.2
	20	492.1	490.0	469.5	492.6
	30	496.9	494.3	472.9	496.8
sub-band		slope [d, e] (K)			
		Mn$_1$-P	Mn$_2$-P	Mn$_3$-P	Mn$_1$-Sb- P
I [c]		-3219.6	-2909.2	-3517.8	-2655.3
II [c]		-2935.1	-3194.2	-3419.9	-2618.4
III [c]		-3001.9	-3205.6	-3516.4	-2611.4

[a] de-convoluted using Gaussian functions. [b] See Fig. S10-S11. [c] See Fig. 6A. [d] via TPD theory. [e] regression factors (R^2) of ≥0.99.

Table S10. Coefficients utilized to simulate H_2O isotherms of the catalysts recorded at 10-40 °C.

catalyst	temperature (°C)	coefficient[a]			regression factor (R^2)
		A (mmol$_{H2O}$ g$_{CAT}^{-1}$)	B (bar^{-1})	C (dimensionless)	
Mn$_1$-P [b]	10	14441.40	0.42×10^{-3}	0.21	0.99
	25	40.95	0.41×10^{-1}	4.01	0.99
	40	8.31	0.15×10^{0}	1.99	0.99
Mn$_2$-P [b]	10	13441.38	0.10×10^{-2}	0.19	0.99
	25	37.95	0.10×10^{0}	4.01	0.99
	40	7.05	0.31×10^{0}	4.01	0.99
Mn$_3$-P [b]	10	13520.57	0.10×10^{-2}	0.19	0.99
	25	37.11	0.11×10^{0}	4.01	0.99
	40	8.38	0.39×10^{0}	4.02	0.99
Mn$_1$-Sb-P [b]	10	14692.74	0.54×10^{-3}	0.22	0.99
	25	54.22	0.60×10^{-2}	4.01	0.99
	40	8.13	0.31×10^{0}	2.02	0.99

[a] via Toth fitting. [b] See Fig. S12.

Table S11. T_{MAX} values and slopes of ln (β/T_{MAX}^2) *versus* $1/T_{MAX}$ for the sub-bands pertaining to the de-convoluted SO$_2$-TPD profiles of the catalysts recorded post SO$_2$ chemisorption at 220 °C with β values of 10-20 °C min^{-1}.

sub-band	β (°C min^{-1})	T_{MAX} (°C)	
		V$_2$O$_5$-WO$_3$	Mn$_1$-Sb-P
I [a, b]	10	473.6	500.0
	15	475.0	501.8
	20	476.1	503.7
II [a, b]	10	608.0	620.0
	15	610.0	622.7
	20	611.6	625.0
III [a, b]	10	685.0	636.7
	15	687.0	639.5
	20	689.2	641.5
IV [a, b]	10	740.5	675.0
	15	743.0	677.8
	20	745.2	680.2
V [a, b]	10	819.2	770.4
	15	822.0	773.6
	20	824.8	776.5

sub-band	slope [d, e] (K)	
	V$_2$O$_5$-WO$_3$	Mn$_1$-Sb-P
I [c]	-6236.2	-4082.5
II [c]	-5720.8	-3765.8
III [c]	-5693.0	-4139.1
IV [c]	-5581.2	-4120.5
V [c]	-5243.0	-4134.5

[a] de-convoluted using Gaussian functions. [b] See Fig. S14. [c] See Fig. 8A. [d] via TPD theory. [e] regression factors (R^2) of ≥0.98.

Table S12. TGA-MASS dataset utilized to assess -r_{ABS} values of the AS/ABS-poisoned catalysts at 260-290 °C.

AS/ABS-poisoned catalyst [a]	$T_{REACTION}$ [b] (°C)	$\Delta T_{REACTION}$ (°C)	Δt (minute)	$\Delta N_{AS/ABS}$ [c, d, e] ($\mu mol_{ABS}\ g_{CAT}^{-1}$)	-r_{ABS} [f] ($\times 10^{-2}\ min^{-1}$)
Mn$_1$-Sb-P	260	0.50	0.10	0.92	7.75
	270	0.35	0.07	0.74	8.86
	280	0.48	0.10	1.11	9.62
	290	0.43	0.09	1.11	10.74
V$_2$O$_5$-WO$_3$	260	0.10	0.02	0.19	4.36
	270	0.08	0.02	0.19	5.26
	280	0.15	0.03	0.38	5.82
	290	0.20	0.04	0.58	6.55

[a] AS/ABS poison environments: 800 ppm NO$_X$; 800 ppm NH$_3$; 500 ppm SO$_2$; 3.0 vol. % O$_2$; 5.4 vol. % H$_2$O; 180 °C; 30 hours; catalysts sieved with sizes of 300-425 μm; GHSV of 60,000 hr^{-1}; total flow rate of 500 mL min^{-1}; balanced by a N$_2$. [b] deviation of <± 0.3 °C from 260-290 °C. [c] AS/ABS pyrolysis environments: total flow rate of 50 mL min^{-1}; ramping rate of 5 °C min^{-1}; under an Ar. [d] presuming the entire transformation of AS into ABS at <260 °C. [e] See Fig. S15. [f] X$_{ABS}$ values of <20.0%.
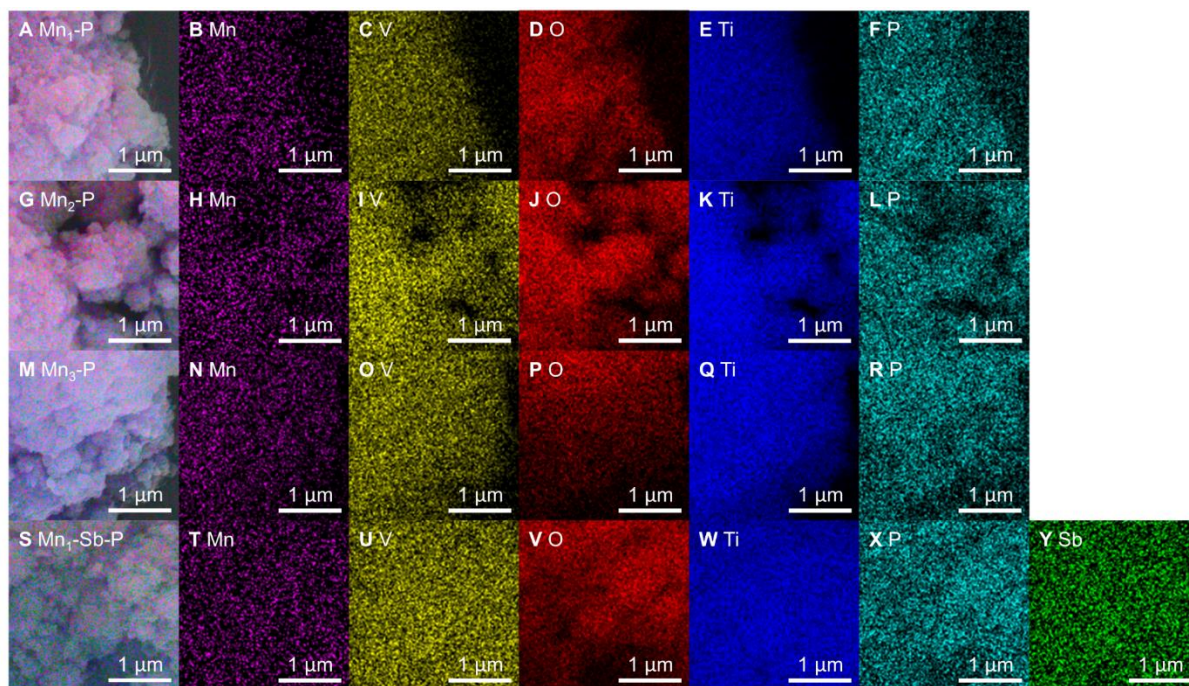
Fig. S1. EDX mapping images of the catalysts (Mn_1-P for (A-F); Mn_2-P for (G-L); Mn_3-P for (M-R); Mn_1-Sb-P for (S-Y)).
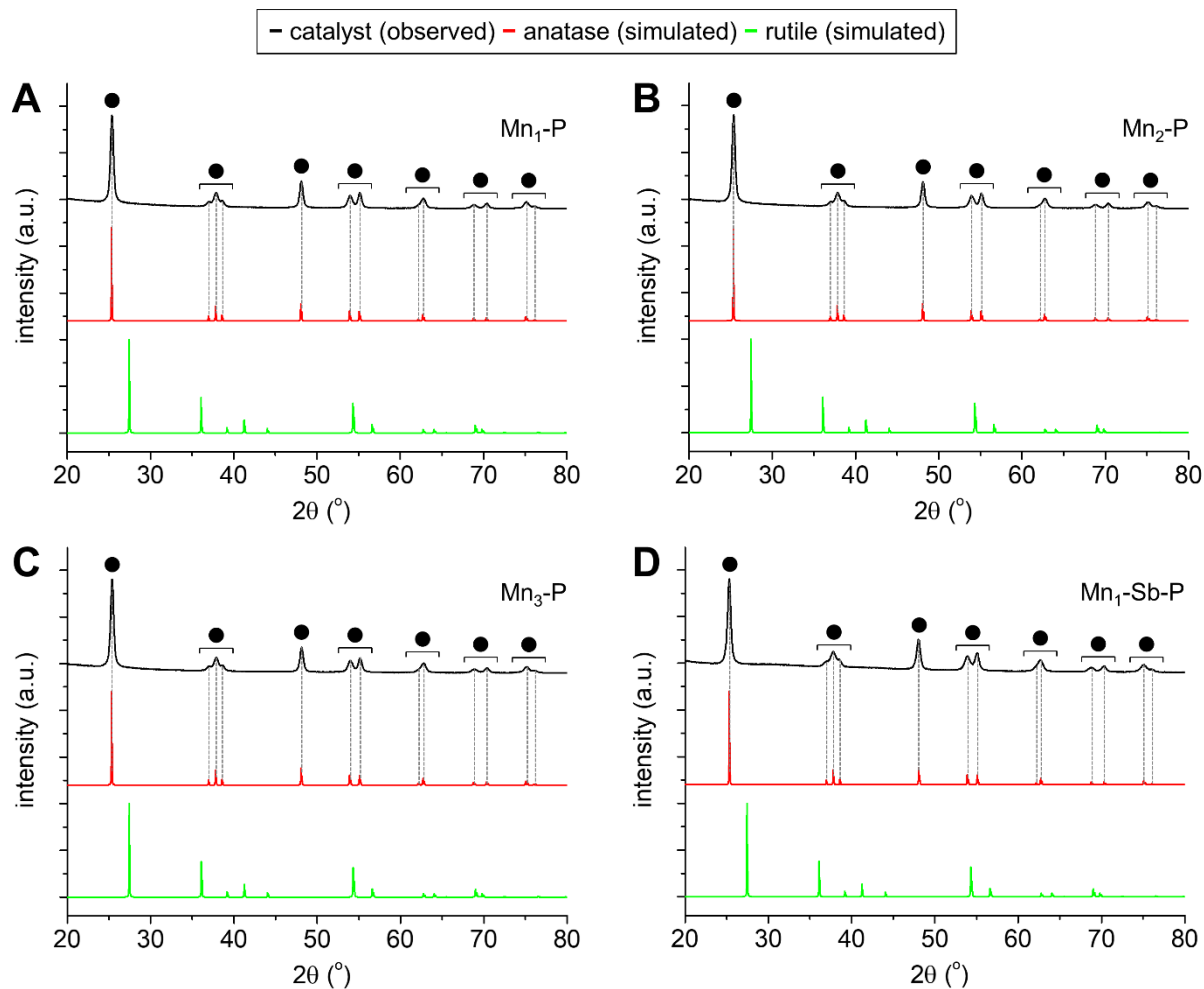
Fig. S2. XRD patterns of the catalysts (black solid lines; Mn$_1$-P for (A); Mn$_2$-P for (B); Mn$_3$-P for (C); Mn$_1$-Sb-P for (D)) and those simulated for *tetragonal* TiO$_2$ polymorphs (red solid lines for anatase (JCPDF No. of 01-071-1166); green solid lines for rutile (JCPDF No. of 01-072-1148)). In (A-D), black solid circles indicate the bulk facets indexed to those for *tetragonal* anatase.
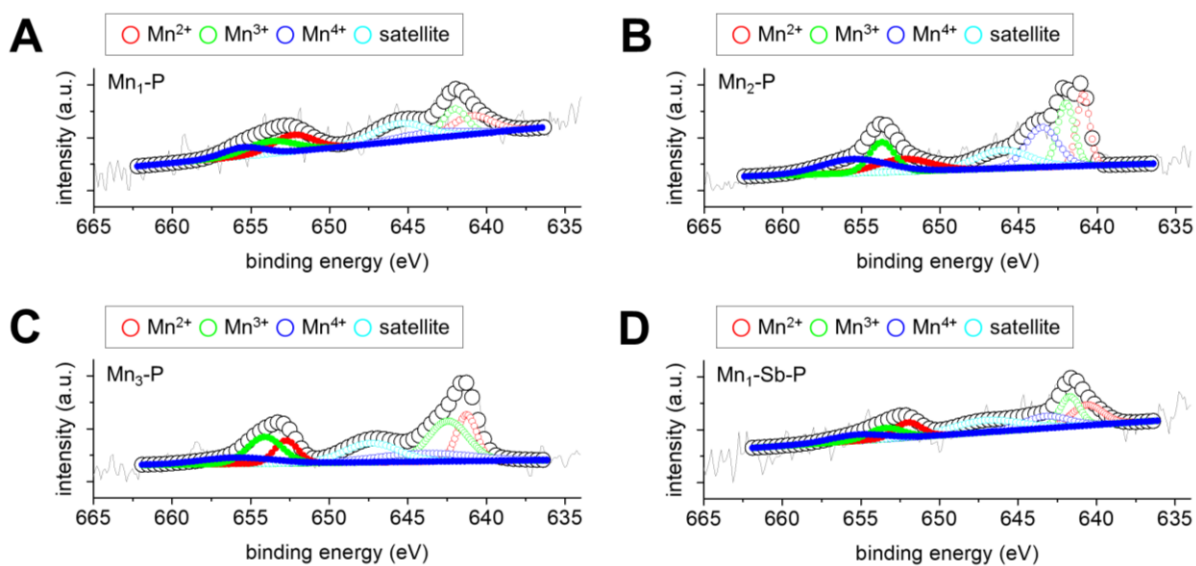
Fig. S3. XP spectra of the catalysts in the Mn 2p regimes (Mn$_1$-P for (A); Mn$_2$-P for (B); Mn$_3$-P for (C); Mn$_1$-Sb-P for (D)). In (A-D), gray solid lines and black empty circles correspond to the raw spectra and those fitted using Gaussian functions, respectively. Moreover, in (A-D), red/green/blue and cyan empty circles indicate surface Mn^{2+}/Mn^{3+}/Mn^{4+} species and satellite positioned in the Mn 2p $_{3/2}$ domains, respectively, whereas red/green/blue solid circles correspond to surface Mn^{2+}/Mn^{3+}/Mn^{4+} species situated in the Mn 2p $_{1/2}$ regions with their relative abundance being detailed in Table S5.
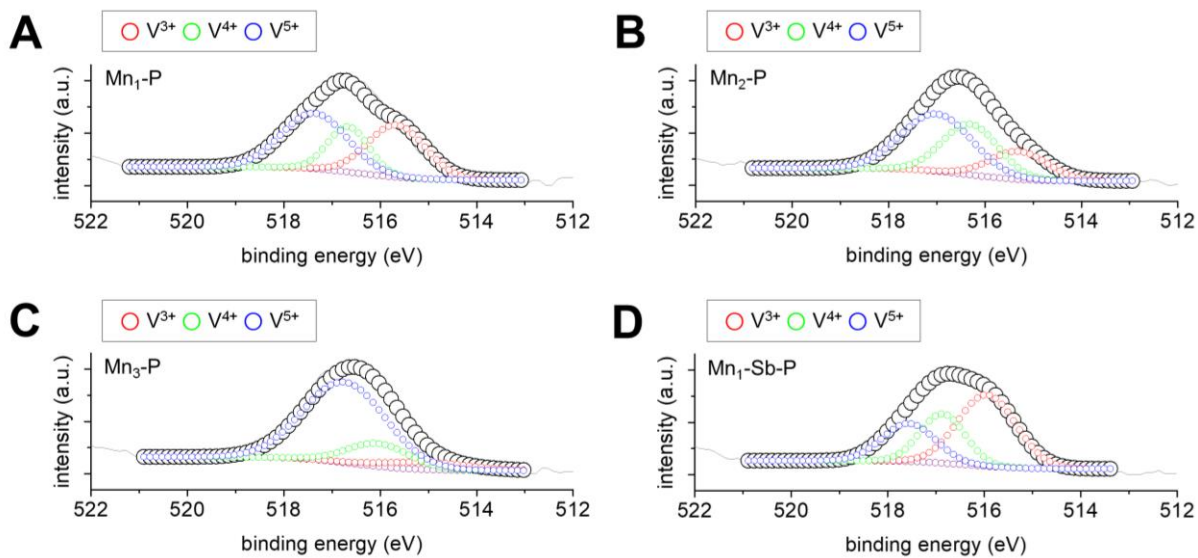
Fig. S4. XP spectra of the catalysts in the V 2p $_{3/2}$ regimes (Mn$_1$-P for (A); Mn$_2$-P for (B); Mn$_3$-P for (C); Mn$_1$-Sb-P for (D)). In (A-D), gray solid lines and black empty circles correspond to the raw spectra and those fitted using Gaussian functions, respectively, whereas red/green/blue empty circles indicate surface V^{3+}/V^{4+}/V^{5+} species with their relative abundance being detailed in Table S5.
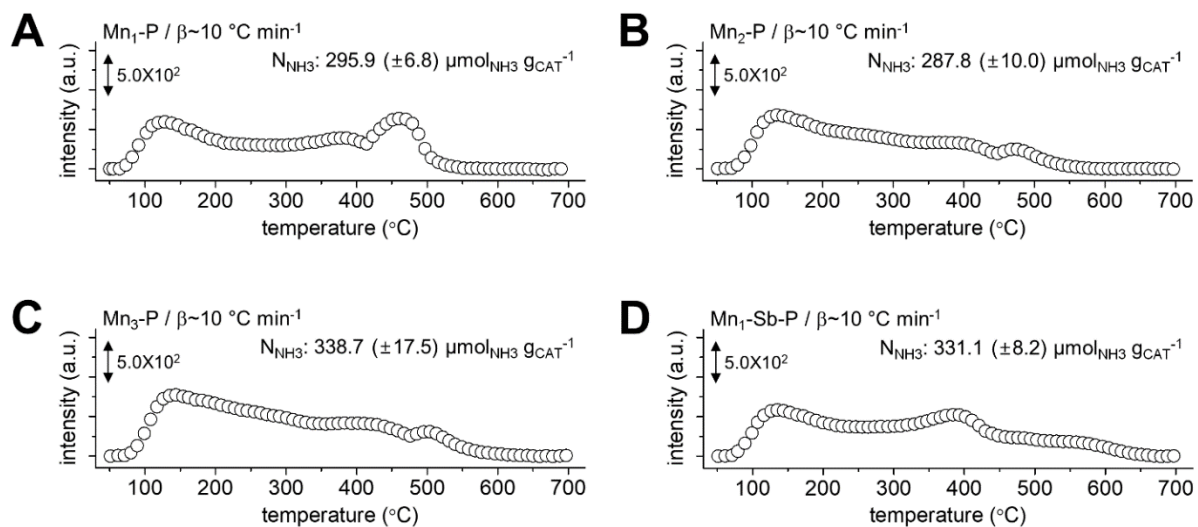
Fig. S5. NH$_3$-TPD profiles (TCD signal *versus* temperature) of the catalysts (Mn$_1$-P for (A); Mn$_2$-P for (B); Mn$_3$-P for (C); Mn$_1$-Sb-P for (D)), whose surfaces chemisorbed NH$_3$ molecules at 50 °C and were heated to 700 °C with a ramping rate (β) of 10 °C min^{-1}. In (A-D), N$_{NH3}$ values indicate the amounts of NH$_3$ chemisorbed in a per-gram of the catalysts at 50 °C.

Fig. S6. NH₃-TPD profiles (TCD signal *versus* temperature) of Mn_1-P (A, C, and E) and Mn_2-P (B, D, and F), whose surfaces chemisorbed NH_3 molecules at 220 °C and were heated to 700 °C with a ramping rate (β) of 10 °C min^{-1} (A-B), 20 °C min^{-1} (C-D), or 30 °C min^{-1} (E-F). In (A-F), N_{NH3} values indicate the amounts of NH_3 chemisorbed in a per-gram of the catalysts at 220 °C. Moreover, in (A-F), NH_3-TPD profiles (black empty circles) were curved-fitted using Gaussian functions to exhibit backgrounds (wine empty circles), sub-band I (red empty circles), sub-band II (green empty circles), and sub-band III (blue empty circles), where sub-band I-III possessed the temperatures with maximum intensities of TCD signals (T_{MAX}). β and T_{MAX} values of sub-band I-III are listed in Table S7 and served to plot ln (β/T_{MAX}^2) *versus* (1/T_{MAX}) for assessing NH_3 binding energies (E_{NH3}) of the catalysts at 220 °C, as shown in Fig. 4A.
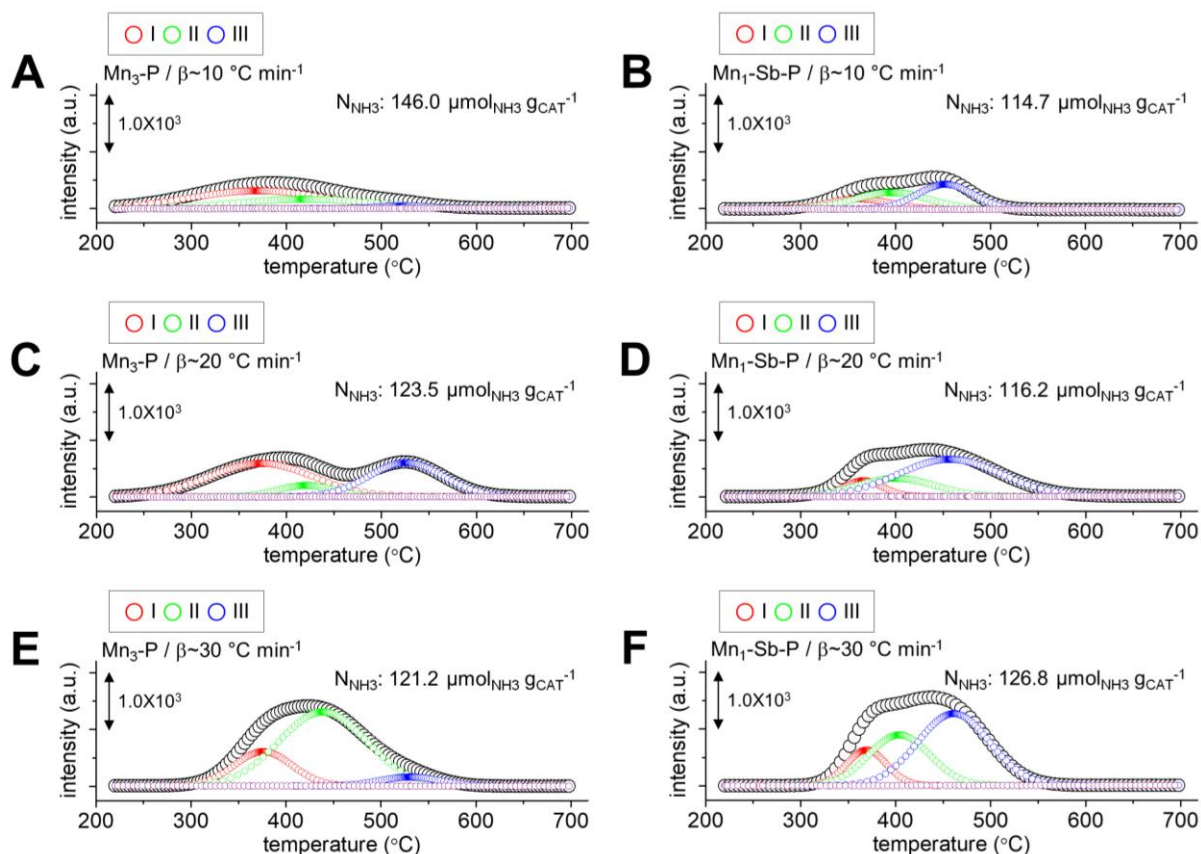
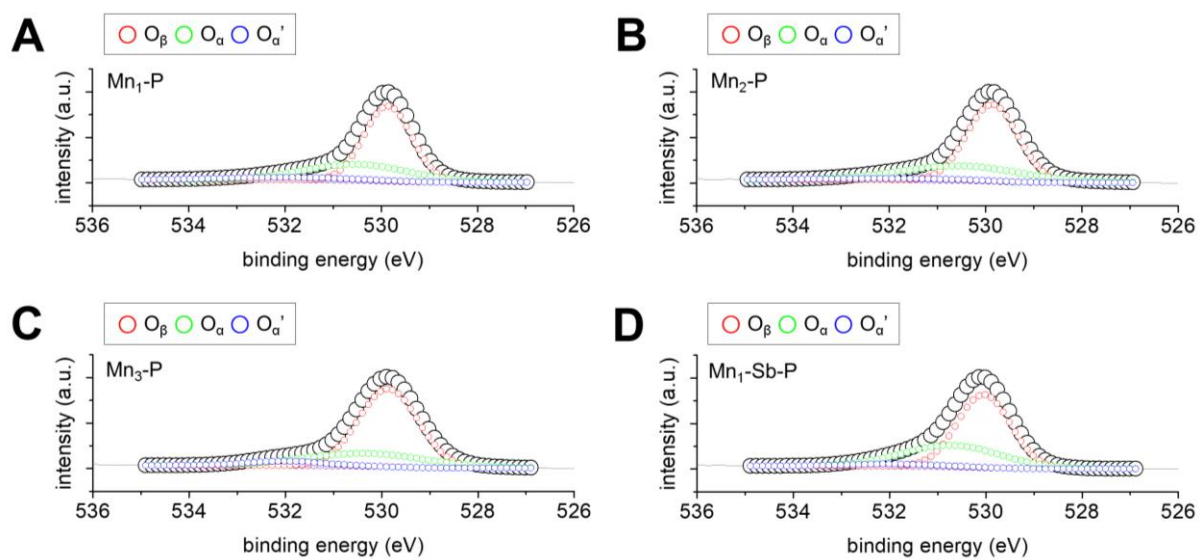**Fig. S7**. NH$_3$-TPD profiles (TCD signal *versus* temperature) of Mn$_3$-P (A, C, and E) and Mn$_1$-Sb-P (B, D, and F), whose surfaces chemisorbed NH$_3$ molecules at 220 °C and were heated to 700 °C with a ramping rate (β) of 10 °C min^{-1} (A-B), 20 °C min^{-1} (C-D), or 30 °C min^{-1} (E-F). In (A-F), N$_{NH3}$ values indicate the amounts of NH$_3$ chemisorbed in a per-gram of the catalysts at 220 °C. Moreover, in (A-F), NH$_3$-TPD profiles (black empty circles) were curved-fitted using Gaussian functions to exhibit backgrounds (wine empty circles), sub-band I (red empty circles), sub-band II (green empty circles), and sub-band III (blue empty circles), where sub-band I-III possessed the temperatures with maximum intensities of TCD signals (T$_{MAX}$). β and T$_{MAX}$ values of sub-band I-III are listed in Table S7 and served to plot ln (β/T$_{MAX}^2$) *versus* (1/T$_{MAX}$) for assessing NH$_3$ binding energies (E$_{NH3}$) of the catalysts at 220 °C, as shown in Fig. 4A.

Fig. S8. XP spectra of the catalysts in the O 1s regimes (Mn_1-P for (A); Mn_2-P for (B); Mn_3-P for (C); Mn_1-Sb-P for (D)). In (A-D), gray solid lines and black empty circles correspond to the raw spectra and those fitted using Gaussian functions, respectively, whereas red/green/blue empty circles indicate surface O_β/O_α/O_α' species with their relative abundance being detailed in Table S5.
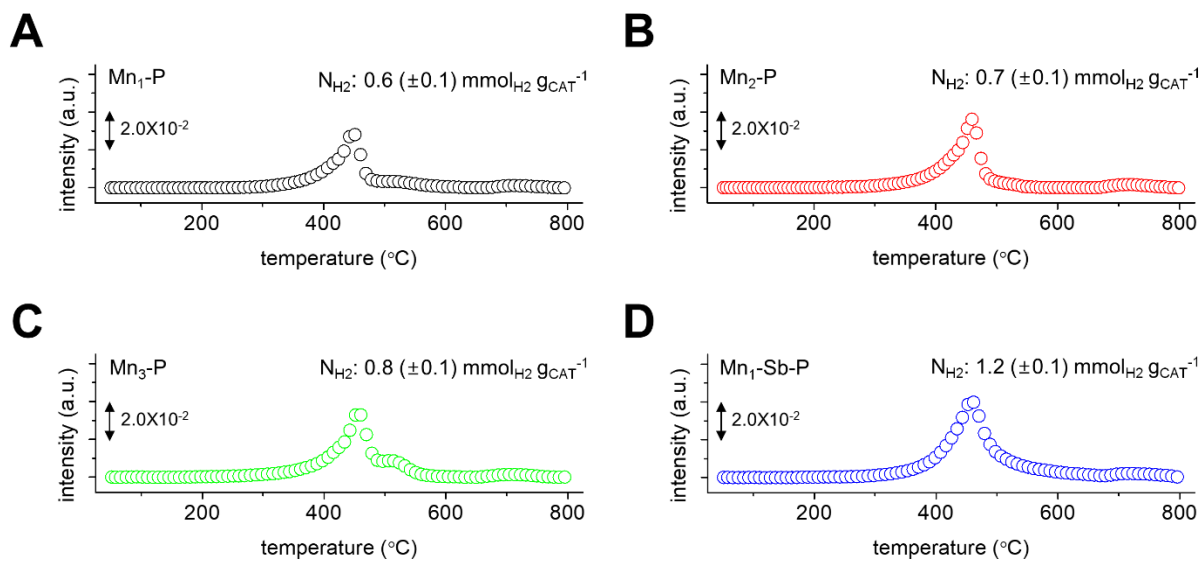
Fig. S9. H_2-TPR profiles (TCD signal *versus* temperature) of the catalysts (Mn_1-P for (A); Mn_2-P for (B); Mn_3-P for (C); Mn_1-Sb-P for (D)), whose surfaces were subjected to H_2 reduction at 50-800 °C with a ramping rate of 10 °C min^{-1}. In (A-D), N_{H2} values indicates the amounts of H_2 needed to reduce the components of the catalysts in use for activating the acidic/redox cycles of the SCR in a per-gram basis.
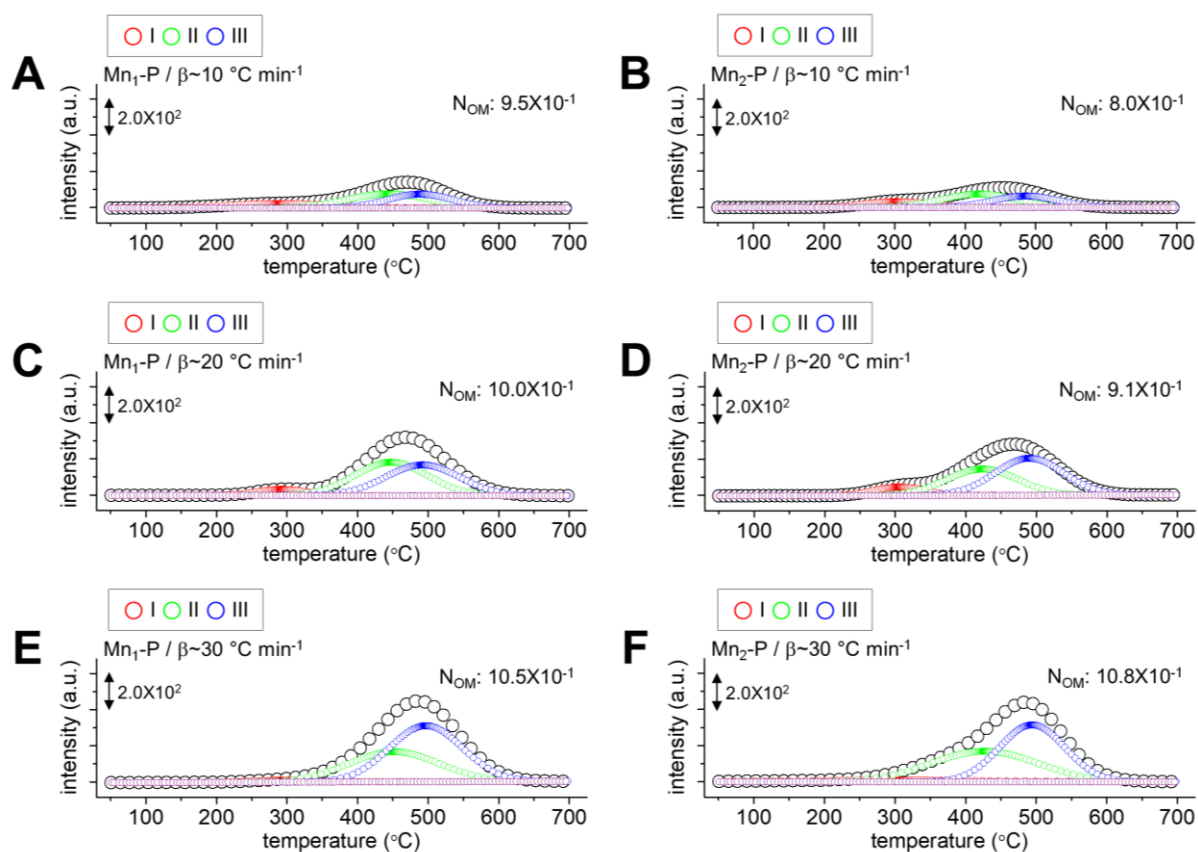
Fig. S10. O$_2$-TPD profiles (TCD signal *versus* temperature) of Mn$_1$-P (A, C, and E) and Mn$_2$-P (B, D, and F), whose surfaces were subjected to H$_2$ reduction at 300 °C with a ramping rate (β) of 10 °C min^{-1} for vacating their O$_V$ sites accessible to O$_M$ species at low temperatures, coordinate O$_M$ (1/2O$_2$) species to O$_V$ sites at 50 °C, and were heated to 700 °C with β value of 10 °C min^{-1} (A-B), 20 °C min^{-1} (C-D), or 30 °C min^{-1} (E-F). In (A-F), N$_{OM}$ values denote the amounts of O$_M$ (1/2O$_2$) species chemisorbed on O$_V$ sites in a per-gram of the catalysts with N$_{OM}$ value of Mn$_1$-P being set as 1.0 at 50 °C. Moreover, in (A-F), O$_2$-TPD profiles (black empty circles) were curved-fitted using Gaussian functions to exhibit backgrounds (wine empty circles), sub-band I (red empty circles), sub-band II (green empty circles), and sub-band III (blue empty circles), where sub-band I-III possessed the temperatures with maximum intensities of TCD signals (T$_{MAX}$). β and T$_{MAX}$ values of sub-band I-III are listed in Table S9 and served to plot ln (β/T$_{MAX}^2$) *versus* (1/T$_{MAX}$) for assessing binding energies between O$_M$ species and O$_V$ sites (E$_{OM}$) for the catalysts at 50 °C, as shown in Fig. 6A.
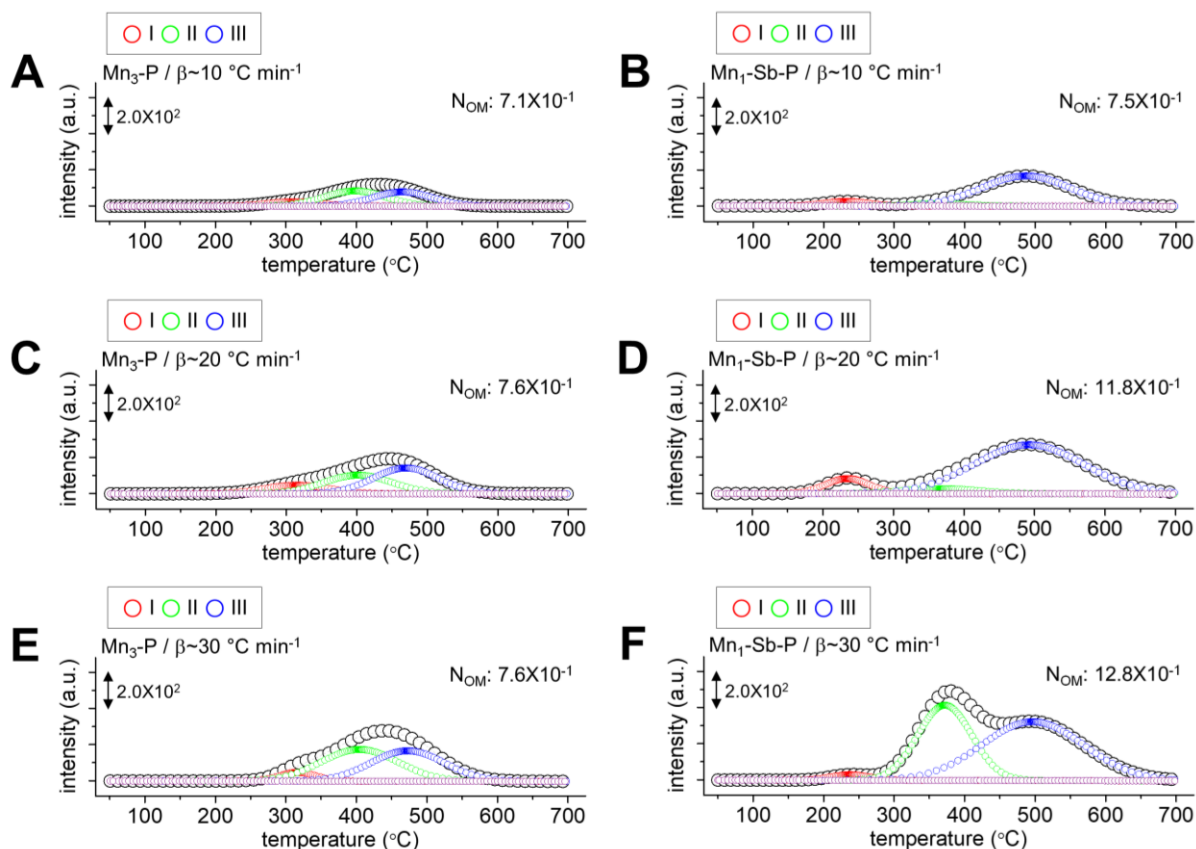
Fig. S11. O$_2$-TPD profiles (TCD signal *versus* temperature) of Mn$_3$-P (A, C, and E) and Mn$_1$-Sb-P (B, D, and F), whose surfaces were subjected to H$_2$ reduction at 300 °C with a ramping rate (β) of 10 °C min^{-1} for vacating their O$_V$ sites accessible to O$_M$ species at low temperatures, coordinate O$_M$ (1/2O$_2$) species to O$_V$ sites at 50 °C, and were heated to 700 °C with β value of 10 °C min^{-1} (A-B), 20 °C min^{-1} (C-D), or 30 °C min^{-1} (E-F). In (A-F), N$_{OM}$ values denote the amounts of O$_M$ (1/2O$_2$) species chemisorbed on O$_V$ sites in a per-gram of the catalysts with N$_{OM}$ value of Mn$_1$-P being set as 1.0 at 50 °C. Moreover, in (A-F), O$_2$-TPD profiles (black empty circles) were curved-fitted using Gaussian functions to exhibit backgrounds (wine empty circles), sub-band I (red empty circles), sub-band II (green empty circles), and sub-band III (blue empty circles), where sub-band I-III possessed the temperatures with maximum intensities of TCD signals (T$_{MAX}$). β and T$_{MAX}$ values of sub-band I-III are listed in Table S9 and served to plot ln (β/T$_{MAX}^2$) *versus* (1/T$_{MAX}$) for assessing binding energies between O$_M$ species and O$_V$ sites (E$_{OM}$) for the catalysts at 50 °C, as shown in Fig. 6A.
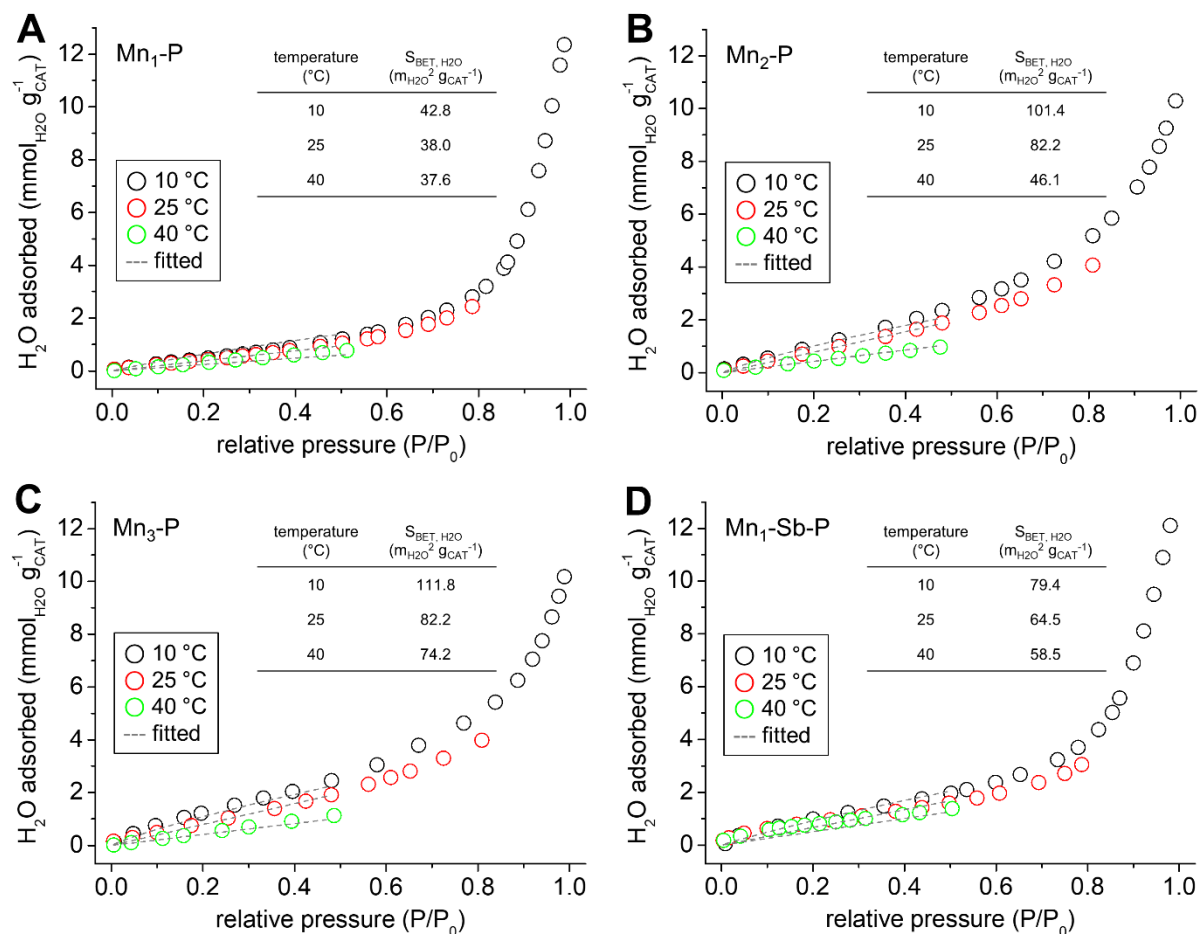
Fig. S12. H_2O adsorption isotherms of the catalysts (Mn_1-P for (A); Mn_2-P for (B); Mn_3-P for (C); Mn_1-Sb-P for (D)) recorded at 10 °C (black empty circles), 25 °C (red empty circles), and 40 °C (green empty circles). H_2O adsorption isotherms of the catalysts were simulated using Toth fitting (gray dashed lines), whose coefficients are specified in Table S10, whereas H_2O-accessible BET surface areas ($S_{BET, H2O}$) of the catalysts at 10-40 °C are listed in inset tables.
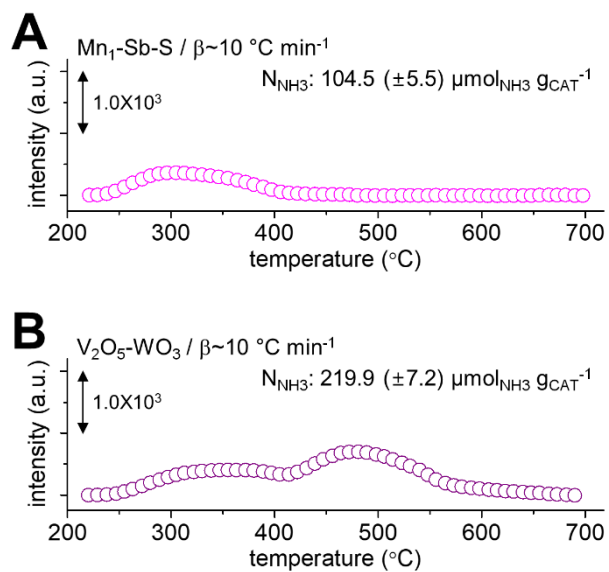
Fig. S13. NH$_3$-TPD profiles (TCD signal *versus* temperature) of Mn$_1$-Sb-S (A) and V$_2$O$_5$-WO$_3$ (B), whose surfaces chemisorbed NH$_3$ molecules at 220 °C and were heated to 700 °C with a ramping rate (β) of 10 °C min^{-1}. In (A-B), N$_{NH3}$ values indicate the amounts of NH$_3$ chemisorbed in a per-gram of the catalysts at 220 °C.
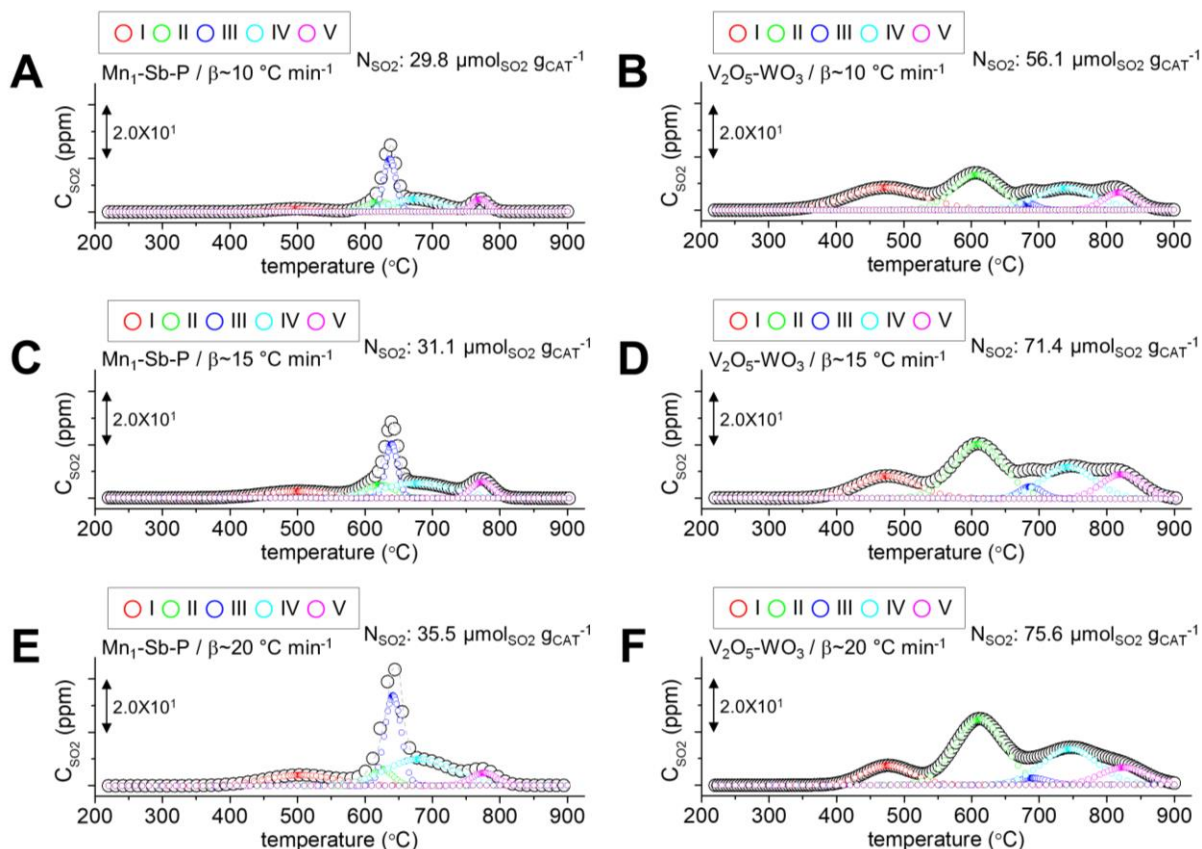
Fig. S14. SO$_2$-TPD profiles (SO$_2$ concentration released (C$_{SO2}$) *versus* temperature) of Mn$_1$-Sb-P (A, C, and E) and V$_2$O$_5$-WO$_3$ (B, D, and F), whose surfaces chemisorbed SO$_2$ molecules at 220 °C and were heated to 900 °C with a ramping rate (β) of 10 °C min^{-1} (A-B), 15 °C min^{-1} (C-D), or 20 °C min^{-1} (E-F). In (A-F), N$_{SO2}$ values indicate the amounts of SO$_2$ chemisorbed in a per-gram of the catalysts at 220 °C. Moreover, in (A-F), SO$_2$-TPD profiles (black empty circles) were curved-fitted using Gaussian functions to exhibit backgrounds (wine empty circles), sub-band I (red empty circles), sub-band II (green empty circles), sub-band III (blue empty circles), sub-band IV (cyan empty circles), and sub-band V (magenta empty circles), where sub-band I-V possessed the temperatures with maximum intensities of C$_{SO2}$ values being released (T$_{MAX}$). β and T$_{MAX}$ values of sub-band I-V are listed in Table S11 and served to plot ln (β/T$_{MAX}^2$) *versus* (1/T$_{MAX}$) for assessing SO$_2$ binding energies (E$_{SO2}$) of the catalysts at 220 °C, as shown in Fig. 8A.
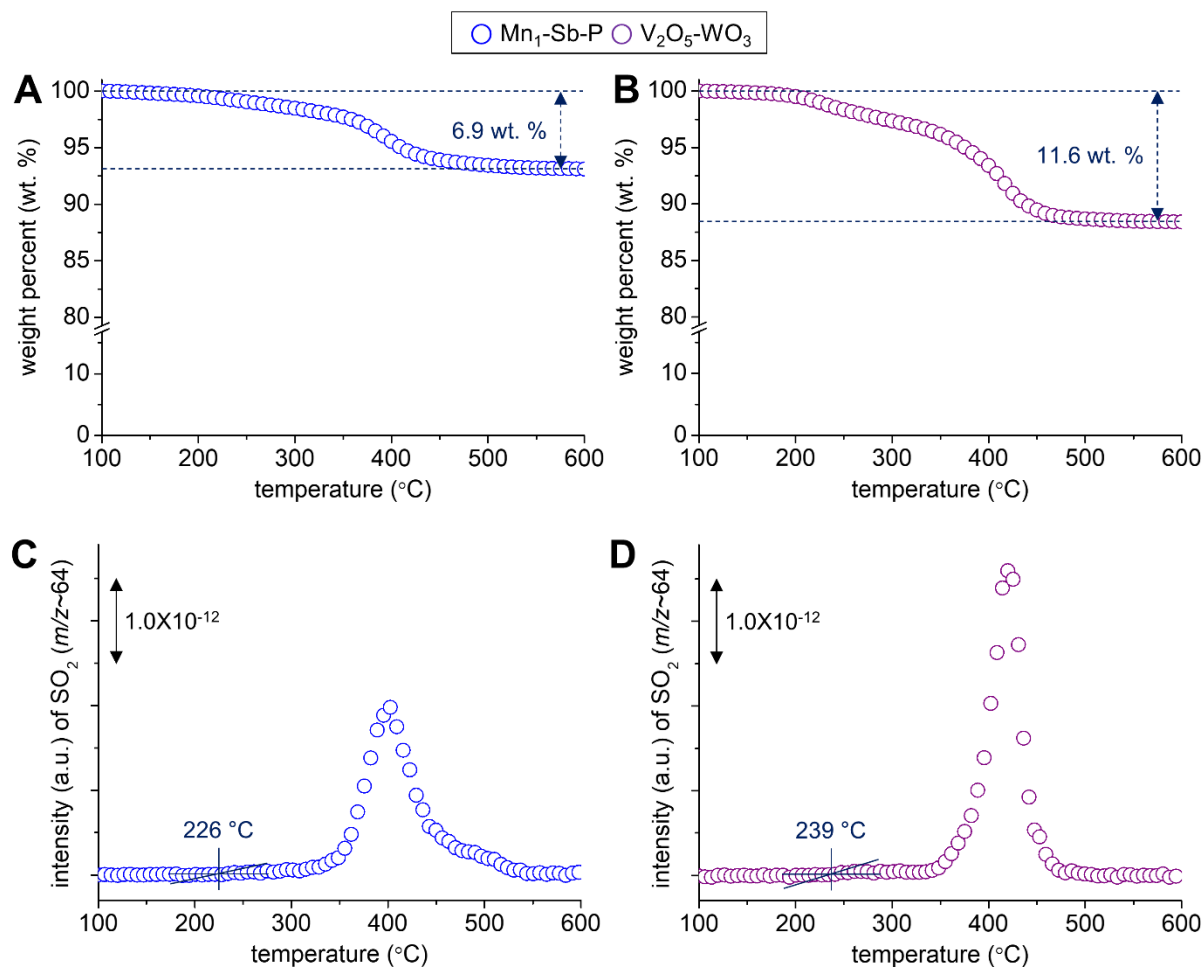
Fig. S15. TGA profiles (weight percent *versus* temperature) of AS/ABS-poisoned Mn_1-Sb-P (A) and V_2O_5-WO_3 (B) under an Ar. In (A-B), values shown with arrows correspond to the quantities of AS/ABS pertaining to the poisoned catalysts. Signals of SO_2 released *versus* temperature for AS/ABS-poisoned Mn_1-Sb-P (C) and V_2O_5-WO_3 (D) subjected to pyrolysis under an Ar. In (C-D), temperatures denote the onsets of SO_2 signal evolution. AS/ABS poison environments: 800 ppm NO_x; 800 ppm NH_3; 500 ppm SO_2; 3.0 vol. % O_2; 5.4 vol. % H_2O; 180 °C; 30 hours; catalysts sieved with sizes of 300-425 μm; GHSV of 60,000 hr^{-1}; total flow rate of 500 mL min^{-1}; balanced by a N_2. AS/ABS pyrolysis environments: total flow rate of 50 mL min^{-1}; ramping rate of 5 °C min^{-1}; under an Ar.
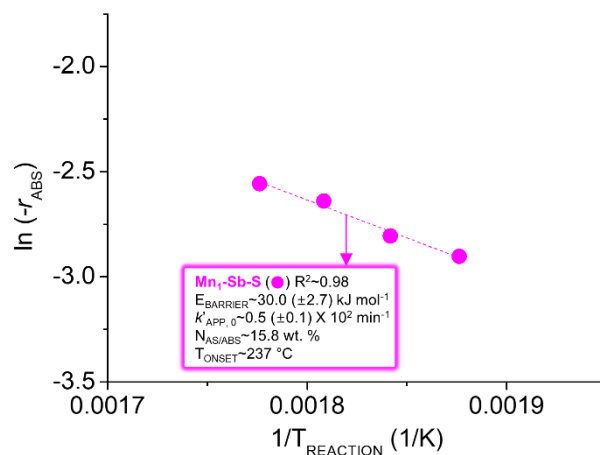
Fig. S16. Arrhenius plot (ln (-r_{ABS}) *versus* 1/$T_{REACTION}$) of Mn_1-Sb-S, where -r_{ABS}, $T_{REACTION}$, R^2, $E_{BARRIER}$/$k'_{APP, 0}$ indicate ABS consumption rate, reaction temperature, regression factor, and energy barrier/lumped collision frequency needed to activate ABS pyrolysis on Mn_1-Sb-S surface, respectively. In addition, $N_{AS/ABS}$ and T_{ONSET} correspond to the amount (wt. %) of AS/ABS inherent to the poisoned Mn_1-Sb-S and the onset of SO_2 signal evolution monitored during ABS pyrolysis of the poisoned Mn_1-Sb-S via TGA-MASS technique, respectively. AS/ABS poison environments: 800 ppm of NO_X; 800 ppm of NH_3; 500 ppm of SO_2; 3.0 vol. % O_2; 7.7 vol. % H_2O; 180 °C; 30 hours; catalysts sieved with sizes of 300-425 μm; space velocity of 60,000 hr^{-1}; total flow rate of 500 mL min^{-1}; balanced by a N_2. AS/ABS pyrolysis environments: total flow rate of 50 mL min^{-1}; ramping rate of 2 °C min^{-1}; under an Ar. Dataset is reprinted in part with permission from ref. [2]. Copyright 2022 American Chemical Society.

References

1. J. Kim, D. H. Kim and H. P. Ha, *J. Hazard. Mater.*, 2020, **397**, 122671.
2. J. Kim, D. H. Kim, J. Park, K. Jeong and H. P. Ha, *ACS Catal.*, 2022, **12**, 2086-2107.
3. S. Lee, J.-H. Lee, H. P. Ha and J. Kim, *Chem. Mater.*, 2022, **34**, 1078-1097.
4. S. Lee, H. P. Ha, J.-H. Lee and J. Kim, *J. Mater. Chem. A*, 2023, **11**, 12062-12079.
5. S. Lee, H. P. Ha, J.-H. Lee and J. Kim, *J. Hazard. Mater.*, 2023, **460**, 132278.
6. S. Lee, J. Choi, H. P. Ha, J.-H. Lee, J. Park and J. Kim, *ACS Catal.*, 2024, **14**, 3349-3368.
7. H. J. An, D. H. Kim, H. P. Ha and J. Kim, *J. Mater. Chem. A*, 2021, **9**, 8350-8371.
8. J. Kim, K. B. Nam and H. P. Ha, *J. Hazard. Mater.*, 2021, **416**, 125780.
9. J. Kim, Y. J. Choe, S. H. Kim, I.-S. Choi and K. Jeong, *JACS Au*, 2021, **1**, 1158-1177.
10. Y. J. Choe, S. H. Kim, K. Jeong and J. Kim, *Chem. Eng. J.*, 2023, **455**, 140537.
11. Y. J. Choe, S. Lee, M. Kim, S. H. Kim, I.-S. Choi, K. Jeong and J. Kim, *Sep. Purif. Technol.*, 2023, **310**, 123146.
12. M. Kim, J. Park, S. H. Kim, J.-H. Lee, K. Jeong and J. Kim, *Carbon*, 2023, **203**, 630-649.
13. M. Kim, M. Al Mamunur Rashid, Y. J. Choe, S. H. Kim, J.-H. Lee, K. Jeong and J. Kim, *J. Mater. Chem. A*, 2023, **11**, 9436-9454.
14. J. Kim, S. Lee and H. P. Ha, *ACS Catal.*, 2021, **11**, 767-786.